BOLETIN DE LA SOCIEDAD ESPAÑOLA DE
Cerámica y Vidrio
www.elsevier.es/bsecv

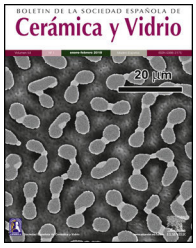

Ablation resistance of graphite coated by spark plasma sintered ZrB_2–SiC based composites

Sadegh Ali Akbarpour Shalmani[a], *Manoochehr Sobhani*[a], *Omid Mirzaee*[a], *Mohammad Zakeri*[b,*]

[a] *Faculty of Materials and Metallurgical Engineering, Semnan University, Semnan, Iran*
[b] *Ceramic Dept, Materials and Energy Research Center, Karaj, Iran*

ARTICLE INFO

Article history:
Received 9 December 2020
Accepted 12 May 2021
Available online 2 June 2021

Keywords:
Coating
Ablation
Graphite
SPS
HfB_2

ABSTRACT

ZrB_2–SiC–HfB_2–WC coating applied by spark plasma sintering led to the ablation resistance improvement of graphite substrate. The influence of HfB_2/WC ratio was investigated on the ablation resistance produced by an oxyacetylene flame. The microstructural evolutions and phase characterization were studied using scanning electron microscopy and X-ray diffraction, respectively. It is confirmed that the ablation resistance of sample with 5% WC and 2.5% HfB_2 was significantly increased with minimum ablated materials and rate of 1.1% and 2.2 mg s^{-1} employing the results of oxyacetylene flame test. The important mechanisms of improvement of the ablation resistance were the evaporation of WO_3 and SiO upon oxidation of SiC and WC in the coating.

Resistencia a la ablación de grafito recubierto por compuestos basados en ZrB_2-SiC sinterizados por plasma de chispa

Palabras clave:
Recubrimiento
Ablación
Grafito
SPS
HfB_2

RESUMEN

El recubrimiento ZrB_2-SiC-HfB_2-WC aplicado mediante sinterización por plasma de chispa condujo a la mejora de la resistencia a la ablación del sustrato de grafito. Se investigó la influencia de la relación HfB_2/WC en la resistencia a la ablación producida por una llama. Las evoluciones microestructurales y la caracterización de fase se estudiaron mediante microscopía electrónica de barrido y difracción de rayos X, respectivamente. Se confirma que la resistencia a la ablación de la muestra con el 5% de WC y el 2,5% de HfB_2 se incrementó significativamente con materiales de ablación mínimos y una tasa del 1,1% y 2,2 mg s^{-1} empleando los resultados de la prueba de llama de oxiacetileno. Los mecanismos importantes de mejora de la resistencia a la ablación fueron la evaporación de WO_3 y SiO tras la oxidación de SiC y WC en el recubrimiento.

* *Corresponding author.*
E-mail address: m_zakeri@merc.ac.ir (M. Zakeri).
https://doi.org/10.1016/j.bsecv.2021.05.004

Introduction

Graphite has important role in structural applications such as rocket, nozzles, turbine, supersonic spacecraft and space shuttle nose operating at high temperatures above 2500 °C [1,2]. These applications are related to the various properties of graphite including high strength at high temperatures, low weight and high thermal stability [3,4]. However it oxidizes at temperatures above 400 °C, therefore, its performance and properties get limited [5,6].

Compounds based on carbides and borides of the transition metals having a melting point above 3000 °C are known as ultra-high temperature ceramics (UHTCs) [7–9]. These materials are favorable candidates for ablation-resistant coating on carbon substrates in harsh condition like aerospace uses [10,11]. UHTC coatings such as SiC (bond coat)/ZrB_2–SiC–$MoSi_2$ [12], SiC/ZrB_2–SiC–Si [13], SiC/ZrC–SiC [14,15] SiC/HfC [16] and SiC/TaC [17] were used to enhance the ablation and oxidation resistance of graphite. Fabrication of these coatings by plasma spraying and pack cementation is costly and time consuming. A porous surface and short cracks with a limited thickness of coating are the results of coatings producing using these techniques (100–500 μm) [18]. UHTCs can be sintered by various fabrication methods like hot-pressing (HP) [19–22], reactive hot-pressing (RHP) [23,24], pressureless sintering (PS) [25–29], and spark plasma sintering (SPS) [30–33].

SPS is a new and fast method used for bonding of dissimilar materials and manufacturing ceramic bulks and coatings [34–36]. This is a modern technique that uses the direct current and uniaxial pressure at the same time to produce the bulk materials. It is used to obtain coating from powders on substrates in less than an hour [37,38]. One of the advantages of SPS is the high heating and cooling rate which results in the formation of dense and fine microstructure [39].

Two-layer coating containing ZrB_2–SiC was used by pressure-assisted diffusion method to ameliorate the oxidation resistance of carbon-carbon composite materials [40]. The results displayed that the multilayer coating makes graphite and carbon-carbon composites resistant to oxidation under high heat flux and high temperature conditions. Passive oxidation layer is formed on the coating surface at high temperature and oxygen pressure and prevents substrate oxidation [40]. Many efforts were performed to enhance the oxidation resistance of zirconium diboride by the introduction of SiC into ZrB_2 [37–41]. In another study, an HfC-SiC coating was manufactured by chemical vapor deposition technique to boost the ablation resistance of carbon-carbon composites. The ablation behavior of the specimens was examined by the oxyacetylene flame. Results demonstrated that the coated specimen shows higher ablation resistance rather than uncoated specimen with a dense microstructure and no crack [16].

SPS process was used to fabricate a dense and thick layer of ZrB_2–SiC–WC coating on the graphite substrate [42]. The results showed that a uniform SiC layer formed at the interface with the main composite top coating and graphite substrate. Moreover, the SiC diffusion zone was formed with appropriate penetration depth in the graphite substrate [42]. In another investigation, the SiC-Si coatings were produced by SPS for improving the ablation resistance of graphite. The results indicated that the increasing SiC leads to the significant improvement of the ablation resistance of the coated graphite [43].

The aim of present research is improvement of the ablation resistance (under oxyacetylene flame) of graphite substrate using the ZrB_2–SiC–HfB_2–WC composite coating by SPS method.

Experimental

ZrB_2 (3 μm, 99.9 wt.%), SiC (10 μm, 99 wt.%), Si (10 μm, 99 wt.%), HfB_2 (5 μm, 99.9 wt.%) and WC (10 μm, 99 wt.%) powders were used for the fabrication of coatings. In all samples, the volumetric percentages of ZrB_2, SiC, Si and sum of HfB_2 + WC were constant and only the ratio of HfB_2 and WC was variable. The chemical compositions of the mixtures made to manufacture each coating are presented in Table 1. The mixture of each coating was prepared after weighing and mixing in an ultrasonic bath (Ethanol media) for 45 min to homogenize it. The obtained suspension was stirred with a magnet device on the heater for 3 h, and finally the suspension was dried at 100 °C for 1 h.

Graphite disks (ø30 mm × 5 mm) with porosity of 14% and density of 1.81 g cm^{-3} were utilized as substrate. Before coating, these disks were grinded (Using SiC abrasive paper ANSI grit size # 320), rinsed with distilled water and dehumidified at 110 °C for 2 h. The inner surface of the SPS die was covered with flexible graphite sheet (Thickness of 1 mm) to minimize its reaction with the coating materials. To fabricate the coatings, the SPS device (SPS-20T-10, China) with a graphite die (diameter of 3 cm) under a pressure of 25 MPa at 1950 °C for 30 min in a vacuum of 15 Pa was used. More details were presented in our previous paper [44].

After soft grinding, microstructural evolutions of the coated specimens were examined using field emission scanning electron microscope (FESEM: Mira3, Tescan, Czech Republic). Energy dispersive spectroscopy (EDS) analysis was employed for the elemental analysis. In order to detect crystalline phases, the X-ray diffractometer (XRD, Bruker/ADVANCE) operating at 45 kV and 40 mA was used. Oxyacetylene flame test (oxidizing condition) was used to investigate the ablation properties of the coated graphite disks. The sample distance to the burner, the heat flux,

Table 1 – The chemical compositions of the mixtures made to manufacture each coating.

Sample Vol.% (Wt.%)	ZrB_2	SiC	Si	HfB_2	WC
A	64.75 (70.18)	13.875 (7.89)	13.875 (5.67)	5 (9.33)	2.5 (6.93)
B	64.75 (69.4)	13.875 (7.8)	13.875 (5.61)	3.75 (6.92)	3.75 (10.28)
C	64.75 (68.63)	13.875 (7.71)	13.875 (5.54)	2.5 (4.56)	5 (13.55)

test time and specimen surface temperature were 15 mm, 8500 W/m^2, 60 s, and 2000 °C, respectively. Ablation rates (R) and weight changes (% ΔW) of the coatings were calculated based on the following formulas:

$$R = \frac{m_0 - m_1}{\Delta t} \quad (1)$$

$$\%\Delta W = \frac{m_0 - m_1}{m_0} \quad (2)$$

where m_0 is the sample weight before and m_1 is the sample weight after the ablation experiment and Δt shows the test time.

Results and discussion

XRD patterns of samples A, B and C were very similar to each other, therefore only one of them (sample C) is shown in Fig. 1. All peaks are related to the starting materials except for Si indicating no reaction between the composite constituents. All samples were hold at 1400 °C for 15 min for complete melting of Si and it's penetrating to the substrate for the formation of SiC. It is clear from the XRD patterns that the Si phase was converted to the SiC during SPS. ZrB_2 and HfB_2 peaks have considerable overlaps and cannot be precisely identified due to their structural similarity. A quadruple composite coating formation on the graphite substrate is confirmed owing to these observations. Adhered graphite on surface of sample is the reason of the graphite peak in the XRD pattern.

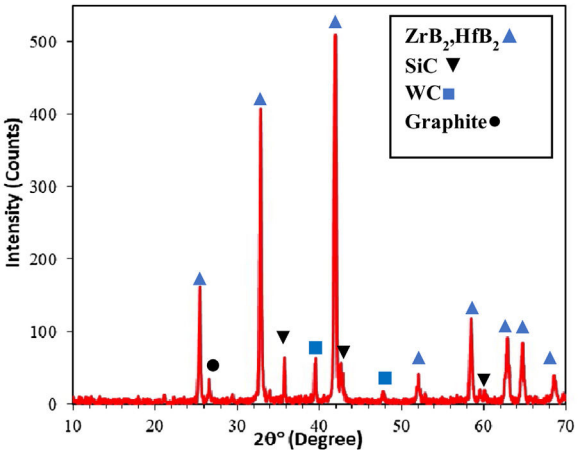

Fig. 1 – XRD pattern of the surface of the coated specimen after SPS.

The microstructures of the coatings cross section are shown in Fig. 2. As it can be seen, it seems that there are three phases, including ZrB_2 (gray zone), SiC (black zone) and

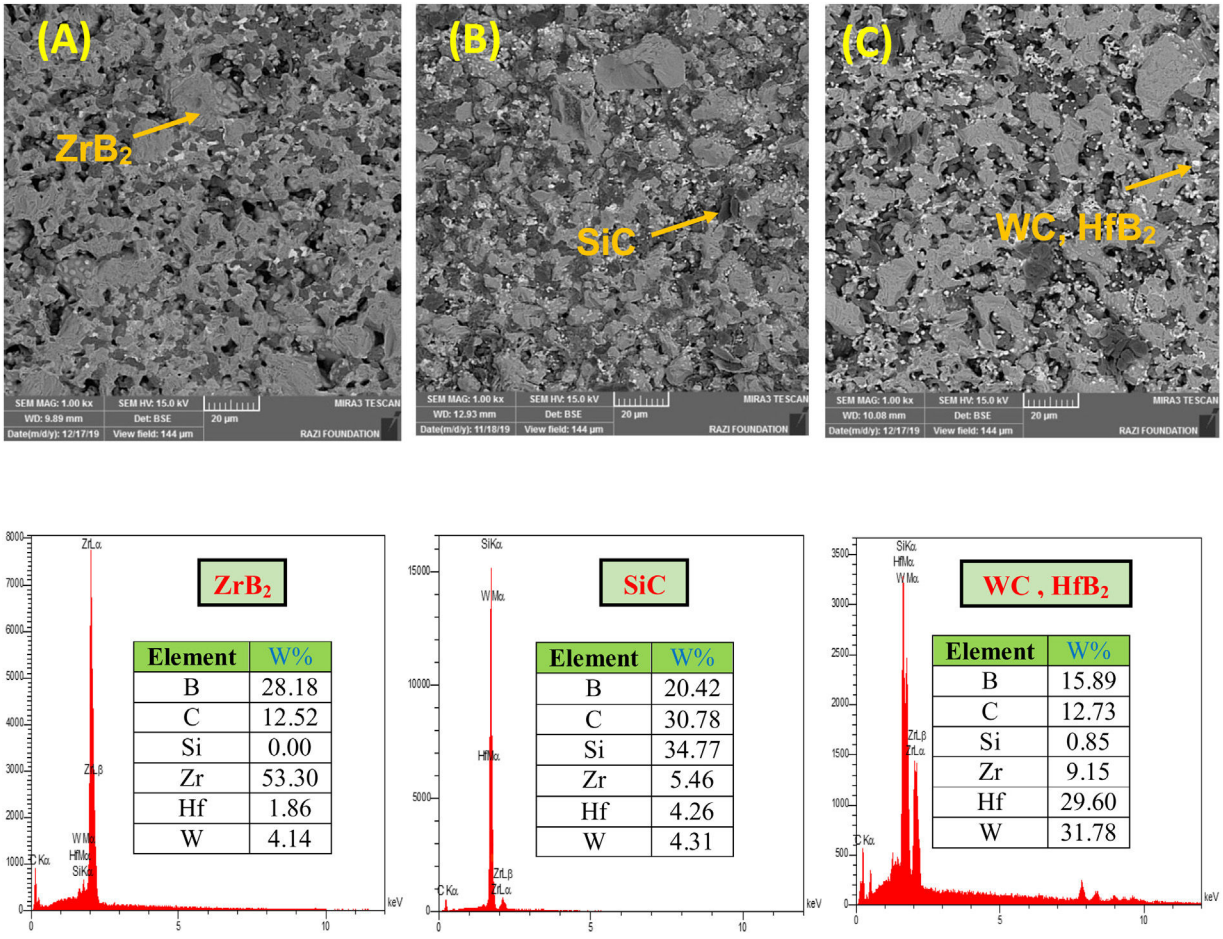

Fig. 2 – SEM images of the cross-section microstructure of: (A) sample A with 2.5%HfB_2–5%WC, (B) sample B with 3.75%HfB_2–3.75%WC, (C) sample C with 5%HfB_2–2.5%WCwith the EDS analysis of marked grains on figure A.

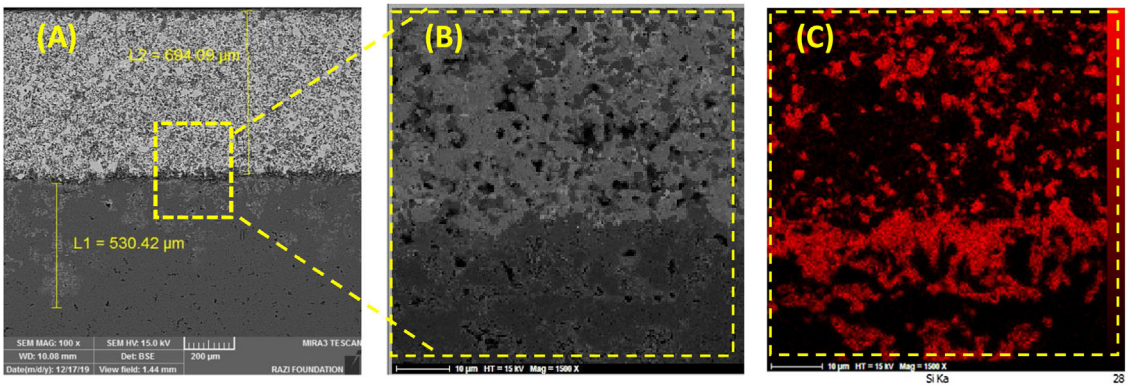

Fig. 3 – SEM image of cross-section of sample C: (A) coating thickness, (B) magnified view of UHTC/graphite interface and (C) MAP of Si measured on B.

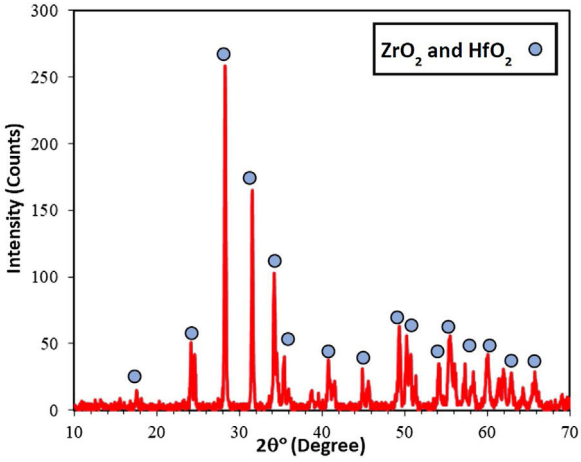

Fig. 4 – XRD pattern of the coating surface after ablation test of sample C.

WC and/or HfB_2 (white zone), in the microstructure of coating according to the EDS spectrum. In contrast, WC and HfB_2 phases appear brighter in the SEM images due to their higher atomic mass and density.

Table 2 – Weight changes and oxidation rates of samples during ablation test.

Sample	ΔW (%)	R (mg s^{-1})
Graphite (no coating)	7.4	7.8
A	2.6	4.4
B	2.0	3
C	1.1	2.2

It is difficult to distinguish them because of their similar atomic mass (WC (195.85 g mol^{-1}) and HfB_2 (200.11 g mol^{-1})). Also according to the EDS analysis, it is clear that the dark grains are SiC phases, because it has low density compared to the other detected phases. The observed higher porosities in Fig. 2A and C can be attributed to the high melting point of HfB_2 (3250 °C) and WC (2870 °C), which can prevent complete sintering of the coatings and lead to porosity formation. According to the higher porosity of sample A compared to sample C, it seems that the presence of HfB_2 retards sintering process. Fig. 3 shows the cross-section of sample C spark plasma sintered at 1950 °C. All coatings were calculated to have a same thickness of 1000 µm before polishing. For the cleaning and removing of the adhered graphite, all sampled were polished to have a same thickness of 700 µm (Fig. 3A). Sample A and B have similar SEM about the penetration depth

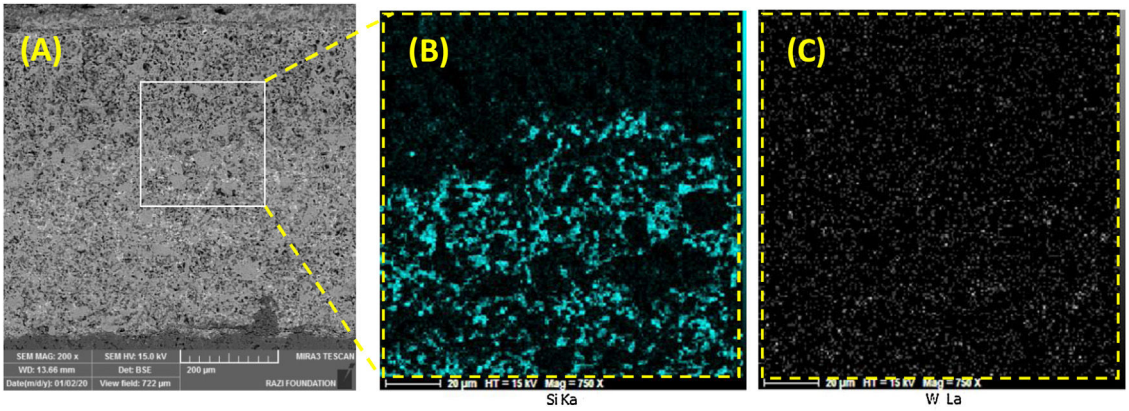

Fig. 5 – (A) SEM image of sample B cross section after oxyacetylene test, (B) Si MAP from the marked square in section A and (C) W MAP as before.

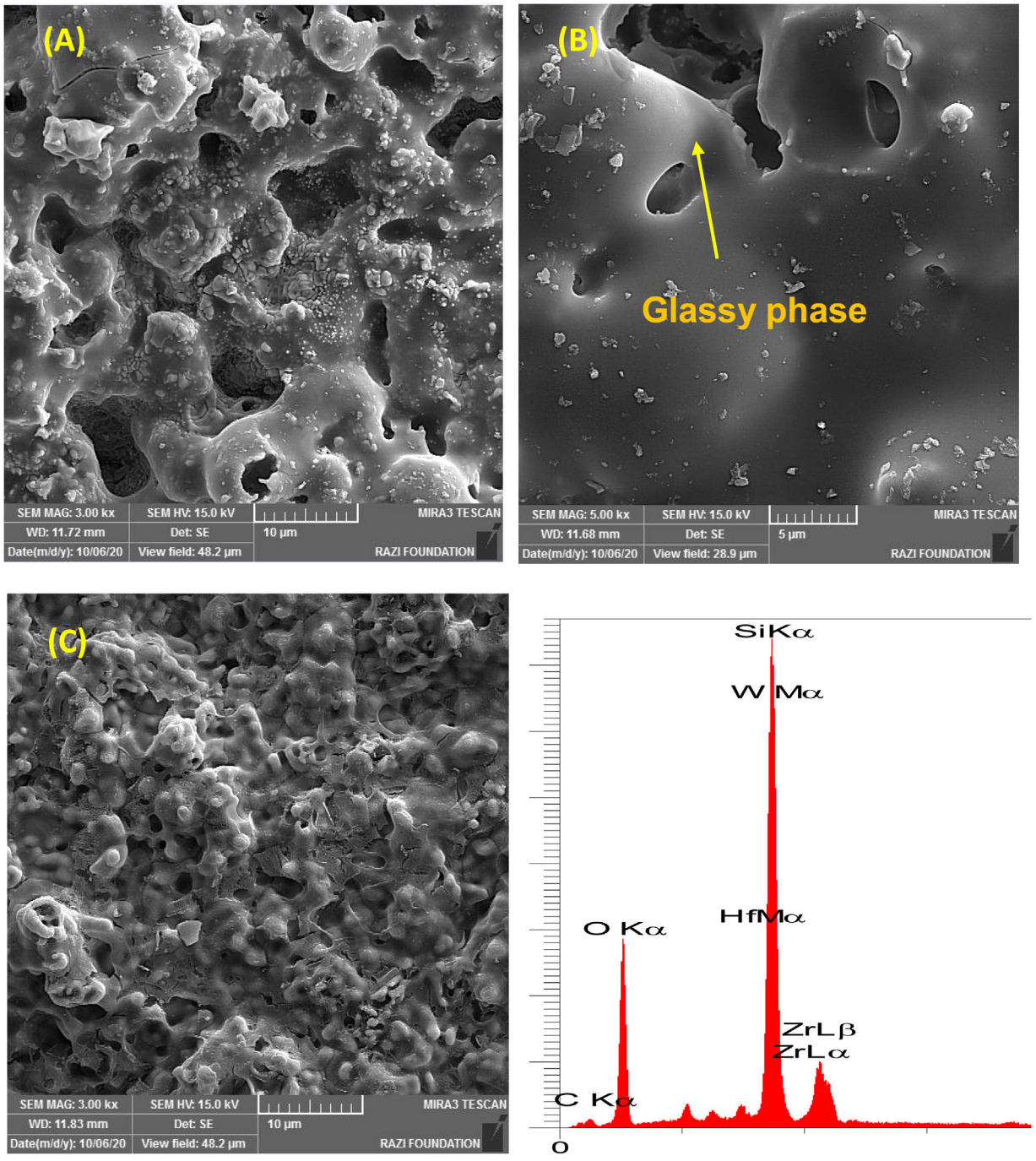

Fig. 6 – SEM images of sample B surface after oxyacetylene test at different magnifications with its EDS analysis.

of Si; therefore their images were not introduced here. It is also observed that the penetration depth of Si into the substrate is up to 500 μm (Fig. 3A) which leads to enhance the adhesion strength. Graphite (substrate) and coating are well interconnected with no crack, porosity, delaminating and other microstructural defects. The formation of SiC phase is due to the diffusion of molten Si into graphite cavities and the chemical reaction between carbon and silicon under the high temperature and pressure of SPS. This secondary SiC phase not only can increase the coating density and strength because of its reaction bonded nature and second, but also it can promote the adhesive strength of coating to the graphite substrate [45]. This dense intermediated layer prevents oxygen diffusion increasing the oxidation resistance. As seen in Fig. 3C, the Si concentration increases from the surface of the coating toward the substrate. In fact, most of the ZrB_2, HfB_2 and WC grains were concentrated on the outside of the coating. On the other hand, SiC was mainly concentrated in the interface between the substrate and the coating.

The high temperature oxyacetylene flame was used to evaluate the ablation resistance of the coatings exposing at 2000 °C for 15 s. Weight changes percentages (ΔW) and ablation rate

(R) of the samples are calculated and presented in Table 2. As seen, ablation resistance of all coated specimens is better than that of uncoated specimens. Sample C had lower ablation rate and higher ablation resistance than samples A and B. XRD analysis related to the surface of sample C after the oxy-acetylene test is shown in Fig. 4. As can be observed, the main phases of the coating are ZrO_2 and HfO_2. Disappearance of the primary phases of composite is related to their oxidation and evaporation according to the following chemical reactions. All thermodynamic data are from reference [46].

$$2ZrB_{2(s)} + 5O_{2(g)} = 2ZrO_{2(s)} + 2B_2O_{3(g)} \quad \Delta G^0_{2000C} = -2326\,kj \quad (3)$$

$$2HfB_{2(s)} + 5O_{2(g)} = 2HfO_{2(s)} + 2B_2O_{3(g)} \quad \Delta G^0_{2000C} = -2349\,kj \quad (4)$$

$$SiC_{(s)} + 2O_{2(g)} = SiO_{2(s)} + CO_{2(g)} \quad \Delta G^0_{2000k} = -1424\,kj \quad (5)$$

$$SiO_{2(s)} + C_{(s)} = SiO_{(g)} + CO_{(g)} \quad \Delta G^0_{2000C} = -164.5\,kj \quad (6)$$

$$2SiO_{2(s)} + SiC_{(s)} = 3SiO_{(g)} + CO_{(g)} \quad \Delta G^0_{2000C} = -251\,kj \quad (7)$$

$$2WC_{(s)} + 5O_{2(g)} = 2WO_{3(g)} + 2CO_{2(g)} \quad \Delta G^0_{2000C} = -1350\,kj \quad (8)$$

As seen all reactions have negative Gibbs free energy; therefore all of them can be performed during ablation test. Fig. 5 shows SEM photographs of the sample B after oxyacetylene test. As discussed before, the SEM images of other samples are very similar together; therefore their images were not introduced here. Due to the emergence of SiC phase in the composite and its oxidation during ablation test (Reaction 3), a glassy high viscous SiO_2 phase is formed. This phase with other oxides (caused by the above reactions) forms a low viscous glassy phase on the surface of coating that prevents oxygen penetration and oxidizing of underlying layer. This glassy phase is shown in Fig. 6. Reaction 4 and 5 leads to the release of SiO and CO gases and consequently creates porosity at the top of the coating. In the next stage, WC oxidation to WO_3 and its evaporation (Reaction 6) absorb the main thermal energy of the flame which prevent the oxidizing and destruction of the main coating structure (ZrB_2 and SiC). Thermal conductivity of HfB_2 (104 w/m k) is higher than ZrB_2 (23–25 w/m k) [47]; therefore it spreads the flame heat throughout the coating and the substrate by increasing the thermal conductivity of the coating which results in the decreasing the overall temperature of the coating. These phenomena promote the ablation resistance of coatings. Owing to the higher ablation resistance of sample C and its higher WC content, it can be concluded that the WC has a greater effect on increasing the composite ablation resistance in comparison to HfB_2.

Conclusion

ZrB_2–SiC–HfB_2–WC composite coatings on the graphite substrate were ideally manufactured by spark plasma sintering. The ablation resistance of the graphite was significantly increased by coatings. However, the composition of the sample C with 5% WC and 2.5% HfB_2 showed the best ablation resistance. Formation of silicate glassy phase in the surface of coating increased the oxidation resistance. The main mechanism of the ablation resistance in these coatings was the formation of WO_3 and SiO gases and their evaporation during heating.

REFERENCES

[1] J.D. Webster, et al., Oxidation protection coatings for C/SiC based on yttrium silicate, J. Eur. Ceram. Soc. 18 (16) (1998) 2345–2350.
[2] A. Lerf, H. He, M. Forster, J. Klinowski, Structure of graphite oxide revisited, J. Phys. Chem. B 102 (23) (1998) 4477–4482.
[3] D.M. Manohar, V. Raju, Effect of pressure and temperature on properties of carbon-carbon composites prepared from renewable material, 2016 International Conference on Control, Computing, Communication and Materials (ICCCCM) (2016) 1–5.
[4] Y. Chu, et al., Oxidation protection of C/C composites with a multilayer coating of SiC and Si+SiC+SiC nanowires, Carbon NY 50 (3) (2012) 1280–1288.
[5] V. Datsyuk, et al., Chemical oxidation of multiwalled carbon nanotubes, Carbon NY 46 (6) (2008) 833–840.
[6] Q. FU, H. LI, X. SHI, K. LI, and G. SUN, Silicon carbide coating to protect carbon/carbon composites against oxidation, Scr. Mater. 52(9) (2005) 923–927.
[7] M. Fattahi, M. Najafi Ershadi, M. Vajdi, F. Sadegh Moghanlou, A. Sabahi Namini, M. Shahedi Asl, On the simulation of spark plasma sintered TiB_2 ultra high temperature ceramics: a numerical approach, Ceram. Int. 46 (10) (2020) 14787–14795.
[8] Z. Ahmadi, B. Nayebi, S. Parvizi, M. Shahedi Asl, M. Shokouhimehr, Phase transformation in spark plasma sintered ZrB_2–V–C composites at different temperatures, Ceram. Int. 46 (7) (2020) 9415–9420.
[9] Z. Ahmadi, M. Zakeri, A. Habibi-Yangjeh, M. Shahedi Asl, A novel ZrB_2–C_3N_4 composite with improved mechanical properties, Ceram. Int. 45 (17) (2019) 21512–21519.
[10] L. Silvestroni, H.-J. Kleebe, W.G. Fahrenholtz, J. Watts, Super-strong materials for temperatures exceeding 2000 °C, Sci. Rep. 7 (1) (2017) 40730.
[11] F. Monteverde, L. Scatteia, Resistance to thermal shock and to oxidation of metal diborides, SiC ceramics for aerospace application, J. Am. Ceram. Soc. 90 (4) (2007) 1130–1138.
[12] Q.-G. Fu, J.-Y. Jing, H.-J. Li, X.-X. Jin, L. Zhuang, L. Li, Design of an inlaid interface structure to improve the oxidation protective ability of SiC–$MoSi_2$–ZrB_2 coating for C/C composites, Ceram. Int. 42 (3) (2016) 4212–4220.
[13] T. Feng, H.-J. Li, M.-H. Hu, H.-J. Lin, L. Li, Oxidation and ablation resistance of Fe_2O_3 modified ZrB_2–SiC–Si coating for carbon/carbon composites, Ceram. Int. 42 (1) (2016) 270–278.
[14] D.-J. Yao, H.-J. Li, H. Wu, Q.-G. Fu, X.-F. Qiang, Ablation resistance of ZrC/SiC gradient coating for SiC-coated carbon/carbon composites prepared by supersonic plasma spraying, J. Eur. Ceram. Soc. 36 (15) (2016) 3739–3746.
[15] X.-H. Shi, et al., Ablation resistance of SiC–ZrC coating prepared by a simple two-step method on carbon fiber reinforced composites, Corros. Sci. 88 (2014) 49–55.
[16] Y.-J. Wang, H.-J. Li, Q.-G. Fu, H. Wu, D.-J. Yao, B.-B. Wei, Ablative property of HfC-based multilayer coating for C/C composites under oxy-acetylene torch, Appl. Surf. Sci. 257 (10) (2011) 4760–4763.
[17] H. Pu, et al., Ablation of vacuum plasma sprayed TaC-based composite coatings, Ceram. Int. 41 (9) (2015) 11387–11395.
[18] Y. Zhang, H. Hu, J. Ren, T. Li, T. Fei, C. Wang, Effect of the surface microstructure of SiC inner coating on the bonding strength and ablation resistance of ZrB_2–SiC coating for C/C composites, Ceram. Int. 42 (16) (2016) 18657–18665.
[19] N. Pourmohammadie Vafa, M. Ghassemi Kakroudi, M. Shahedi Asl, Advantages and disadvantages of graphite

addition on the characteristics of hot-pressed ZrB_2–SiC composites, Ceram. Int. 46 (7) (2020) 8561–8566.
[20] M. Shahedi Asl, M. Ghassemi Kakroudi, Characterization of hot-pressed graphene reinforced ZrB_2–SiC composite, Mater. Sci. Eng. A 625 (2015) 385–392.
[21] M. Shahedi Asl, M. Ghassemi Kakroudi, R. Abedi Kondolaji, H. Nasiri, Influence of graphite nano-flakes on densification and mechanical properties of hot-pressed ZrB2–SiC composite, Ceram. Int. 41 (4) (2015) 5843–5851.
[22] T.P. Nguyen, et al., Influence of SiAlON addition on the microstructure development of hot-pressed ZrB_2–SiC composites, Ceram. Int. 46 (11) (2020) 19209–19216.
[23] N.P. Vafa, M. Shahedi Asl, M. Jaberi Zamharir, M. Ghassemi Kakroudi, Reactive hot pressing of ZrB_2-based composites with changes in ZrO_2/SiC ratio and sintering conditions. Part I: Densification behavior, Ceram. Int. 41 (7) (2015) 8388–8396.
[24] N. Pourmohammadie Vafa, B. Nayebi, M. Shahedi Asl, M. Jaberi Zamharir, M. Ghassemi Kakroudi, Reactive hot pressing of ZrB_2-based composites with changes in ZrO2/SiC ratio and sintering conditions. Part II: Mechanical behavior, Ceram. Int. 42 (2) (2016) 2724–2733.
[25] C. Xia, et al., Electron microscopy study of ZrB_2–SiC–AlN composites: hot-pressing vs. pressureless sintering, Ceram. Int. (2020).
[26] V.-H. Nguyen, et al., Electron microscopy characterization of porous ZrB_2–SiC–AlN composites prepared by pressureless sintering, Ceram. Int. (2020).
[27] M. Khoeini, A. Nemati, M. Zakeri, M. Shahedi Asl, Pressureless sintering of ZrB_2 ceramics codoped with TiC and graphite, Int. J. Refract. Met. Hard Mater. 81 (2019) 189–195.
[28] M. Shahedi Asl, B. Nayebi, Z. Ahmadi, P. Pirmohammadi, M. Ghassemi Kakroudi, Fractographical characterization of hot pressed and pressureless sintered SiAlON-doped ZrB_2–SiC composites, Mater. Charact. 102 (2015) 137–145.
[29] Z. Ahmadi, B. Nayebi, M. Shahedi Asl, M. Ghassemi Kakroudi, I. Farahbakhsh, Sintering behavior of ZrB_2–SiC composites doped with Si_3N_4: a fractographical approach, Ceram. Int. 43 (13) (2017) 9699–9708.
[30] Z. Ahmadi, B. Nayebi, M. Shahedi Asl, I. Farahbakhsh, Z. Balak, Densification improvement of spark plasma sintered TiB_2-based composites with micron-, submicron- and nano-sized SiC particulates, Ceram. Int. 44 (10) (2018) 11431–11437.
[31] Z. Balak, M. Zakeri, M. Rahimipour, E. Salahi, Taguchi design and hardness optimization of ZrB_2-based composites reinforced with chopped carbon fiber and different additives and prepared by SPS, J. Alloys Compd. 639 (2015) 617–625.
[32] Z. Hamidzadeh Mahaseni, M. Dashti Germi, Z. Ahmadi, M. Shahedi Asl, Microstructural investigation of spark plasma sintered TiB_2 ceramics with Si_3N_4 addition, Ceram. Int. 44 (11) (2018) 13367–13372.
[33] A. Babapoor, M.S. Asl, Z. Ahmadi, A.S. Namini, Effects of spark plasma sintering temperature on densification, hardness and thermal conductivity of titanium carbide, Ceram. Int. 44 (12) (2018) 14541–14546.
[34] M. Vajdi, F. Sadegh Moghanlou, Z. Ahmadi, A. Motallebzadeh, M. Shahedi Asl, Thermal diffusivity and microstructure of spark plasma sintered TiB_2–SiC–Ti composite, Ceram. Int. 45 (7) (2019) 8333–8344.
[35] F. Adibpur, S.A. Tayebifard, M. Zakeri, M. Shahedi Asl, Spark plasma sintering of quadruplet ZrB_2–SiC–ZrC–Cf composites, Ceram. Int. 46 (1) (2020) 156–164.
[36] Y. Pazhouhanfar, A. Sabahi Namini, S. Shaddel, Z. Ahmadi, M. Shahedi Asl, Combined role of SiC particles and SiC whiskers on the characteristics of spark plasma sintered ZrB_2 ceramics, Ceram. Int. 46 (5) (2020) 5773–5778.
[37] Z.A. Munir, U. Anselmi-Tamburini, M. Ohyanagi, The effect of electric field and pressure on the synthesis and consolidation of materials: a review of the spark plasma sintering method, J. Mater. Sci. 41 (3) (2006) 763–777.
[38] E.A. Olevsky, S. Kandukuri, L. Froyen, Consolidation enhancement in spark-plasma sintering: impact of high heating rates, J. Appl. Phys. 102 (11) (2007) 114913.
[39] H. Istgaldi, M. Shahedi Asl, P. Shahi, B. Nayebi, Z. Ahmadi, Solid solution formation during spark plasma sintering of ZrB_2–TiC–graphite composites, Ceram. Int. 46 (3) (2020) 2923–2930.
[40] E.L. Corral, R.E. Loehman, Ultra-high-temperature ceramic coatings for oxidation protection of carbon–carbon composites, J. Am. Ceram. Soc. 91 (5) (2008) 1495–1502.
[41] A.L. Chamberlain, W.G. Fahrenholtz, G.E. Hilmas, D.T. Ellerby, Characterization of zirconium diboride for thermal protection systems, Key Eng. Mater. 264–268 (2004) 493–496.
[42] M. Shirani, M. Rahimipour, M. Zakeri, S. Safi, T. Ebadzadeh, ZrB_2–SiC–WC coating with SiC diffusion bond coat on graphite by spark plasma sintering process, Ceram. Int. 43 (16) (2017) 14517–14520.
[43] F. Golestani, M. Zakeri, M. Razavi, M.R. Rahimipour, M. Shirani, Microstructure and ablative properties of Si–SiC coating prepared by spark plasma sintering, Ceram. Int. 44 (7) (2018) 8403–8408.
[44] S. Ali Akbarpour Shalmania, M. Sobhani, O. Mirzaee, M. Zakeri, Effect of HfB_2 and WC additives on the ablation resistance of ZrB_2–SiC composite coating manufactured by SPS, Ceram. Int. 46 (2020) 25106–25112.
[45] S. Safi, A. Kazemzadeh, MCMB–SiC composites; new class high-temperature structural materials for aerospace applications, Ceram. Int. 39 (1) (2013) 81–86.
[46] Ihsan Barin, Thermochemical Data of Pure Substances, ISBN 3-527-28745-0, Third Edition, 1995.
[47] Gasch, M.J., D.T. Ellerby, and S.M. Johnson, Ultra High Temperature Ceramic Composites. 2005, NASA Glenn Research Center, USA: Kluwer Academic Publishers. 554.